AGU PUBLICATIONS

JGR

Journal of Geophysical Research: Atmospheres

RESEARCH ARTICLE
10.1002/2014JD021644

**Key Points:**
- Improved $NO_x$ emission inversion by coupling with satellite retrieval
- More consistent inversion results between using GOME-2 and OMI measurements
- Significant seasonal and weekly variations of $NO_x$ emission in China

**Supporting Information:**
- Readme
- Figure S1
- Figure S2
- Figure S3

**Correspondence to:**
Y. Wang,
yuhang.wang@eas.gatech.edu

**Citation:**
Gu, D., Y. Wang, C. Smeltzer, and K. F. Boersma (2014), Anthropogenic emissions of $NO_x$ over China: Reconciling the difference of inverse modeling results using GOME-2 and OMI measurements, *J. Geophys. Res. Atmos.*, *119*, doi:10.1002/2014JD021644.

Received 18 FEB 2014
Accepted 30 MAY 2014
Accepted article online 3 JUN 2014

# Anthropogenic emissions of $NO_x$ over China: Reconciling the difference of inverse modeling results using GOME-2 and OMI measurements

**Dasa Gu[1], Yuhang Wang[1], Charles Smeltzer[1], and K. Folkert Boersma[2,3]**

[1]School of Earth and Atmospheric Sciences, Georgia Institute of Technology, Atlanta, Georgia, USA, [2]Climate Observations Department, Royal Netherlands Meteorological Institute, De Bilt, Netherlands, [3]Department of Meteorology and Air Quality, Wageningen University, Wageningen, Netherlands

**Abstract** Inverse modeling using satellite observations of nitrogen dioxide ($NO_2$) columns has been extensively used to estimate nitrogen oxides ($NO_x$) emissions in China. Recently, the Global Ozone Monitoring Experiment-2 (GOME-2) and Ozone Monitoring Instrument (OMI) provide independent global $NO_2$ column measurements on a nearly daily basis at around 9:30 and 13:30 local time across the equator, respectively. Anthropogenic $NO_x$ emission estimates by applying previously developed monthly inversion (MI) or daily inversion (DI) methods to these two sets of measurements show substantial differences. We improve the DI method by conducting model simulation, satellite retrieval, and inverse modeling sequentially on a daily basis. After each inversion, we update anthropogenic $NO_x$ emissions in the model simulation with the newly obtained a posteriori results. Consequently, the inversion-optimized emissions are used to compute the a priori $NO_2$ profiles for satellite retrievals. As such, the a priori profiles used in satellite retrievals are now coupled to inverse modeling results. The improved procedure was applied to GOME-2 and OMI $NO_2$ measurements in 2011. The new daily retrieval-inversion (DRI) method estimates an average $NO_x$ emission of 6.9 Tg N/yr over China, and the difference between using GOME-2 and OMI measurements is 0.4 Tg N/yr, which is significantly smaller than the difference of 1.3 Tg N/yr using the previous DI method. Using the more consistent DRI inversion results, we find that anthropogenic $NO_x$ emissions tend to be higher in winter and summer than spring (and possibly fall) and the weekday-to-weekend emission ratio tends to increase with $NO_x$ emission in China.

## 1. Introduction

Nitrogen oxides ($NO_x = NO + NO_2$) play a key role in the formation of ozone and secondary aerosols. $NO_x$ is emitted from both anthropogenic sources (e.g., fossil fuel combustion and human-induced biomass burning) and natural sources (e.g., lightning, wildfires, and soil emissions). One region that has witnessed rapid changes in $NO_x$ emissions in the past two decades is China. These changes have been reported previously in analyses of satellite-measured tropospheric nitrogen dioxide ($NO_2$) columns [e.g., *Ghude et al.*, 2009; *Gu et al.*, 2013; *Ma et al.*, 2006; *Richter et al.*, 2004; *Uno et al.*, 2007; *van der A et al.*, 2006].

The traditional bottom-up inventories of $NO_x$ emissions, estimated from limited information of emission source factors and statistical data over China, could have large uncertainties [e.g., *Ohara et al.*, 2007; *Streets et al.*, 2003]. On the basis of the relationship between local emission and tropospheric $NO_2$ column simulated by a chemical transport model, inverse modeling has been used to combine bottom-up inventories with top-down constraints from satellite column $NO_2$ observations, such as Global Ozone Monitoring Experiment (GOME), Scanning Imaging Absorption Spectrometer for Atmospheric Chartography (SCIAMACHY), Ozone Monitoring Instrument (OMI), and Global Ozone Monitoring Experiment-2 (GOME-2), in order to reduce uncertainties in $NO_x$ emission estimations [e.g., *Choi et al.*, 2012; *Han et al.*, 2009; *He et al.*, 2007; *Kunhikrishnan et al.*, 2004; *Kurokawa et al.*, 2009; *Lin et al.*, 2012; *Martin et al.*, 2003; *Richter et al.*, 2005; *Shi et al.*, 2008; *Stavrakou et al.*, 2008; *Zhang et al.*, 2012].

*Martin et al.* [2003] developed the first monthly inversion (MI) method by combining the bottom-up emission inventory with top-down constraints from GOME $NO_2$ column measurements. The method was extended by *Zhao and Wang* [2009] to carry out the emission inversion iteratively on a daily basis to account in part for the nonlinear effects in chemical feedbacks. One issue that has not been discussed extensively is that the inverse modeling that results from different satellites can differ significantly; part of the issue is attributable to a priori profiles used in retrievals [e.g., *Irie et al.*, 2012; *Lin et al.*, 2010; *Vinken et al.*, 2014]. We choose to use

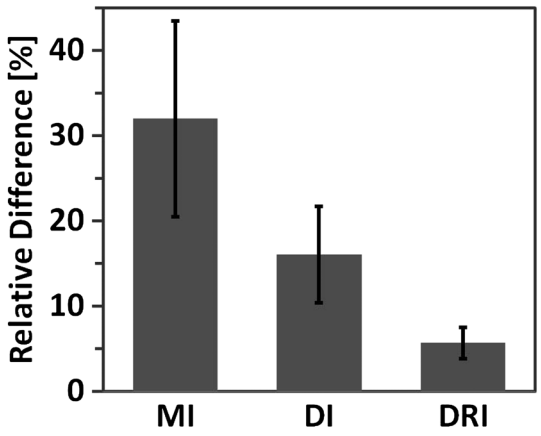


**Figure 1.** Relative difference between GOME-2 and OMI measurement constrained anthropogenic $NO_x$ emission estimates over China using MI [*Martin et al.*, 2003], DI [*Zhao and Wang*, 2009], and improved DRI methods for 2011. The vertical bar shows 1σ uncertainty.

GOME-2 and OMI measurements in this study because these two instruments have a similar temporal sampling frequency that is substantially better than SCIAMACHY. Figure 1 compares the inverse modeling results of anthropogenic $NO_x$ emissions between using GOME-2 and OMI measurements. Satellite measurements, a priori emissions, and the regional chemical and transport model used in the comparison will be discussed in the next section. By applying the MI method [*Martin et al.*, 2003] with simulations from the Regional Chemical and Transport Model (REAM), we find that the relative difference of $NO_x$ inversion emission estimates between using GOME-2 and OMI measurements is $32 \pm 12\%$ over China in 2011. The difference is reduced to $16 \pm 6\%$ by using the daily inversion (DI) method [*Zhao and Wang*, 2009], but it remains very large. The substantial difference of inverse modeling results from the two sets of satellite measurements raises an obvious question of consistency in potential science applications of these emission estimates. While not solving the problem, the iteration in the DI method helps reduce the difference compared to MI method. In this study, we examine if the difference can be further reduced by improving the inverse modeling method. We improve the DI method by updating on a daily basis anthropogenic $NO_x$ emissions in REAM using the inversion results and subsequently the a priori $NO_x$ profiles used in the satellite retrieval. The improved daily retrieval-inversion (DRI) method therefore couples the retrieval profiles to inverse modeling results and ensures the consistency between them. The DRI method is applied in the REAM model to improve surface anthropogenic $NO_x$ emission estimates with GOME-2 and OMI measurements over China in 2011. The DRI inversion results are compared to those using the DI method to demonstrate the benefits of the new method. We analyze further the seasonal and weekday-to-weekend variations of anthropogenic $NO_x$ emissions over China using the new DRI inversion products.

## 2. Satellite Observations and Inverse Modeling Methods

### 2.1. GOME-2 and OMI Tropospheric $NO_2$ Columns

Both GOME-2 and OMI instruments are nadir-viewing spectrometers [e.g., *Boersma et al.*, 2004, 2007, 2011]. The OMI instrument was launched onboard the Aura satellite in July 2004, and it has a spatial resolution of $24 \times 13\ km^2$ at nadir [*Levelt et al.*, 2006]. The GOME-2 instrument was launched onboard the METOP-A satellite in October 2006 with ground pixel size of $80 \times 40\ km^2$ [*Irie et al.*, 2012]. The local equator crossing time is around 9:30 for GOME-2 and around 13:30 for OMI. We excluded the data in all flagged rows with anomalies for the OMI measurements (http://www.knmi.nl/omi/research/product/rowanomaly-background.php). In addition, we only use measured $NO_2$ column data when cloud fraction is $< 30\%$ for both instruments.

In MI and DI inversions, we use the Royal Netherlands Meteorological Institute (KNMI) OMI (DOMINO2 v2.0) and GOME-2 (TM4NO2A v2.3) tropospheric $NO_2$ vertical column density (VCD) products [*Boersma et al.*, 2004, 2007]. Comparing these two products, the GOME-2 VCDs are significantly higher than OMI VCDs up to $>110\%$ over eastern China in 2011 (Figure S1 in the supporting information). Higher GOME-2 VCD values reflect a longer chemical lifetime of $NO_x$ in midmorning than the OMI observation time of early afternoon [e.g., *Irie et al.*, 2012].

In the DRI method, we recompute tropospheric $NO_2$ VCD data using OMI or GOME-2 measurements. In order to maintain consistency in comparison, we use the KNMI algorithm in the retrievals of both OMI and GOME-2 tropospheric $NO_2$ VCDs [*Boersma et al.*, 2011]. The retrieval procedure includes estimation of $NO_2$ slant column density (SCD), calculation of tropospheric SCD by subtracting the TM4 assimilated stratospheric column, and converting the tropospheric SCD into VCD with the tropospheric air mass factor (AMF). The tropospheric AMF

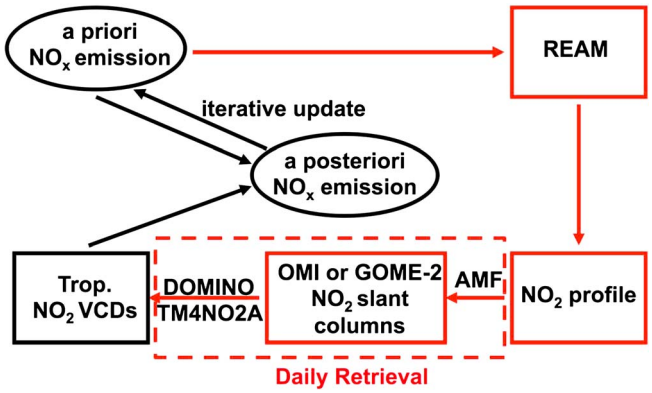


**Figure 2.** Schematic diagrams of the DI (in black arrows) and new DRI (in red arrows) methods. In the DRI method, the daily iterative update includes $NO_x$ emissions, $NO_2$ profiles, and tropospheric $NO_2$ VCD retrievals. In the DI method, only $NO_x$ emissions are updated daily. In the DRI method, satellite $NO_2$ SCD products are used; In the DI method, KNMI DOMINO2 and TM4NO2A tropospheric $NO_2$ VCD products are used.

calculation depends on a priori tropospheric $NO_2$ profile, surface albedo, cloud pressure, cloud fraction, and satellite-viewing geometry. A more detailed description can be found in *Boersma et al.* [2007]. In the MI and DI methods [*Martin et al.*, 2003; *Zhao and Wang*, 2009], the model simulation of a priori tropospheric profiles is decoupled from inverse modeling. In other words, the emissions used in the model and retrieval are not necessarily consistent with the inverse modeling results. We solve this problem in the DRI method by updating the model emissions and the a priori profiles using inverse modeling results on a daily basis (to be shown in Figure 2).

The error in the retrieval of $NO_2$ tropospheric VCD is determined by those in total SCD, stratospheric SCD, and tropospheric AMF estimation. In this study, we use total and stratospheric SCD errors from KNMI DOMINO2 and TM4NO2A products and compute the error of tropospheric AMF estimation following the KNMI algorithm. The details of error analysis were described by *Boersma et al.* [2004, 2007, 2011] and *Hains et al.* [2010]. In general, the errors of total and stratospheric SCD estimations are relatively small ($<0.7\times10^{15}$ molecules $cm^{-2}$) relative to high tropospheric VCDs ($>10\times10^{15}$ molecules $cm^{-2}$) over eastern China [*Zhao and Wang*, 2009]. The error in tropospheric AMF comes from surface albedo, cloud fraction, cloud pressure, and profile shape. The total error per retrieval is ~30% over most areas in China for both OMI and GOME-2.

### 2.2. REAM Model

The 3-D REAM has been applied in a number of tropospheric chemistry and transport studies over East Asia, North America, and polar regions [e.g., *Choi et al.*, 2005, 2008a, 2008b; *Jing et al.*, 2006; *Liu et al.*, 2010, 2012a, 2012b; *Wang et al.*, 2006, 2007; *Yang et al.*, 2011; *Zeng et al.*, 2003, 2006; *Zhao and Wang*, 2009; *Zhao et al.*, 2009a, 2009b, 2010]. The model has a horizontal resolution of $70\times70$ $km^2$ with 21 vertical layers in the troposphere. Transport is driven by Weather Research and Forecasting (WRF) model assimilated meteorological fields constrained by the National Centers for Environmental Prediction (NCEP) reanalysis products (http://www.esrl.noaa.gov/psd/). The chemistry mechanism in REAM is adopted from the GEOS-Chem model [*Bey et al.*, 2001] with updates of kinetics data (http://jpldataeval.jpl.nasa.gov/). The anthropogenic $NO_x$ and VOCs emissions are from *Zhang et al.* [2009]. The biomass burning emissions are taken from the Global Fire Emissions Database, Version 2 (GFEDv2.1) (available at http://daac.ornl.gov/). The lightning $NO_x$ emission is parameterized by *Zhao et al.* [2010].

### 2.3. Inverse Modeling

The MI method for anthropogenic $NO_x$ emissions and uncertainties based on bottom-up and top-down constraints was developed by *Martin et al.* [2003]. We compared the emission estimates by using the DI method [*Zhao and Wang*, 2009] with that using the MI method based on KNMI DOMINO2 and TM4NO2A products in Figure 1. The improvement in annualized difference from 32% (MI) to 16% (DI) is significant. However, the difference in the DI method can still reach to >32% on a monthly basis (to be shown in Figure 4).

In the DI method, only $NO_x$ emission is computed iteratively on a daily basis (Figure 2). In this method, which largely follows *Martin et al.* [2003], a top-down emission is estimated by scaling the a priori emission with the ratio of observed and simulated tropospheric $NO_2$ column. The a posteriori emission is then calculated by error-weighted averaging of the a priori and top-down emissions (the error distributions of the a priori $NO_x$ and the top-down $NO_x$ estimates are assumed to be lognormal). The optimized a posteriori emission and its errors are then used as the a priori in the next day. The whole process iterates daily at the satellite overpass time.

One potential problem in the DI method is that the vertical profiles used in the retrieval are not necessarily consistent with the a posteriori emissions. For example, an increase of emissions will generally increase the

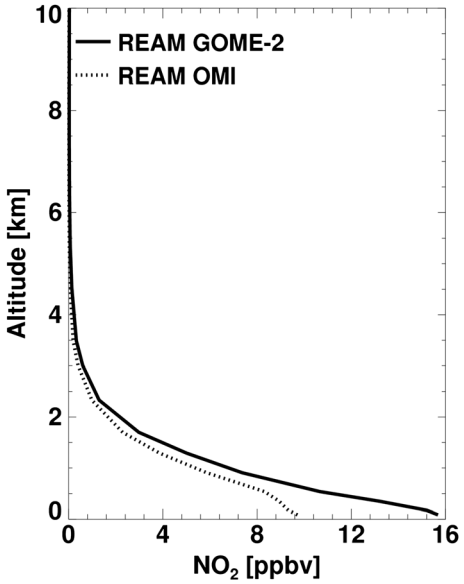


**Figure 3.** Simulated monthly mean $NO_2$ vertical profiles over Bijing in the DRI method at GOME-2 and OMI local overpass times for March 2011.

vertical gradient of $NO_2$ profiles and change the AMF values used in the retrieval of tropospheric $NO_2$ column (section 2.1). Furthermore, when we compare the inverse modeling results from two satellite measurements, additional inconsistency can be introduced if the model used to compute $NO_2$ profiles in AMF calculation is different from the model used in inverse modeling. Figure 3 shows REAM-simulated monthly mean $NO_2$ profiles at GOME-2 and OMI overpass times for March, which has the largest monthly mean difference between DI inversion results using KNMI DOMINO2 OMI and TM4NO2A GOME-2 tropospheric $NO_2$ VCD products for 2011 (to be shown in Figure 4). The vertical gradient of $NO_2$ in the lower troposphere is greater for GOME-2 than OMI since GOME-2 overpass is in midmorning while OMI overpass is in early afternoon. We did not show in the figure the corresponding profiles from TM4, which are used in the KNMI products, since the TM4 profiles for GOME-2 retrievals were not archived.

In the DRI method, we improve $NO_x$ inverse modeling by updating the emissions from the inversion results and subsequently the a priori $NO_2$ profiles used in the satellite retrieval on a daily basis (Figure 2). Tropospheric $NO_2$ columns are retrieved online daily before inverse modeling. Tropospheric AMFs are first computed with REAM-simulated $NO_2$ profiles and then used in retrieval process to derive tropospheric $NO_2$ VCD from GOME-2 or OMI $NO_2$ SCD. The online-computed tropospheric $NO_2$ VCD is subsequently applied in inverse modeling to estimate the a posteriori emissions and errors. After the inversion, the optimized a posteriori emissions and errors are then used as the a priori data in subsequent model simulation, satellite retrieval, and inverse modeling. Therefore, we ensure consistency between the a posteriori emissions and the $NO_2$ profiles used in GOME-2 and OMI retrievals.

The uncertainties of the a posteriori emissions are derived from those in a priori and top-down emission estimates. Uncertainties in top-down emission estimates come from those in tropospheric $NO_2$ VCD retrievals and model simulations. The retrieval error is discussed in section 2.1. The uncertainty of model simulation is estimated at 30% and that of the bottom-up inventory is ~60% over China [*Zhao and Wang*, 2009]. The overall uncertainties of the a posteriori emission are typically in the range of 20–40% over polluted eastern China (Figure S2 in the supporting information).

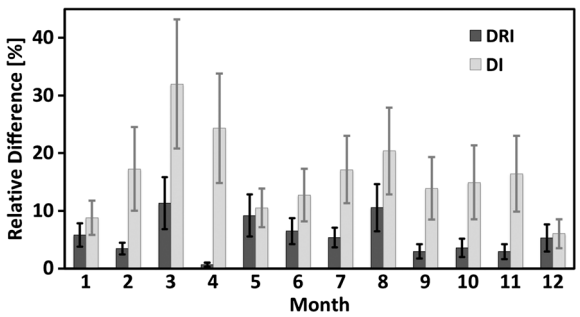


**Figure 4.** Relative differences of monthly anthropogenic $NO_x$ emission estimates over China between GOME-2 and OMI measurement-based inversion results using DRI (black) and DI (grey) methods for 2011. The vertical bars show 1σ uncertainty.

## 3. Results and Discussions

### 3.1. Comparison Between GOME-2 and OMI Measurement Based Inversion Results

We showed in Figure 1 the yearly relative difference between GOME-2 and OMI measurement based inversion results for $NO_x$ emissions over China using the MI and DI methods, respectively. The DI method reduces the annual mean $NO_x$ emission difference between OMI and GOME-2 based inversion results to 16 ± 6% from 32 ± 12% of the MI method. However, the monthly difference is still quite large in DI method, ranging from <10% in December and

January to > 30% in March (Figure 4). The newly developed DRI method, on the other hand, reduces the difference consistently every month compared to the DI method. The maximum difference, which is in March, is reduced to < 12%. The annual mean difference decreases to 5 ± 2%.

Figure S1 in the supporting information compares tropospheric $NO_2$ VCDs between KNMI DOMINO2 OMI and TM4NO2A GOME-2 products and those retrieved by DRI. While the chemical lifetime difference reflected in part in the difference between $NO_2$ vertical profiles at GOME-2 and OMI observation times (Figure 3) and it is expected to yield higher $NO_2$ VCDs at GOME-2 observation time than OMI, the column difference is clearly much larger between KNMI DOMINO2 OMI and TM4NO2A GOME-2 products than between the corresponding DRI retrievals. A close inspection reveals that the differences between KNMI and DRI tropospheric VCDs are much larger for GOME-2 than OMI. The main reason is that KNMI GOME-2 tropospheric VCD estimates are much larger than DRI results. The difference between KNMI and DRI OMI products is much smaller in comparison. Since the TM4 profiles used in KNMI GOME-2 retrievals were not archived, we cannot compare TM4 profiles to those from REAM.

While the total a posteriori emissions over China in the DRI method are in good agreement between using OMI and GOME-2 measurements, regional differences still exist. Figure 5 (top row) shows the annual mean a posteriori $NO_x$ emissions over China for 2011 by using DRI method with GOME-2 measurements. There are high $NO_x$ emissions in economically developed eastern and southern China. Comparing the a posteriori $NO_x$ emissions from the two satellites, we find much larger differences in a posteriori $NO_x$ emission estimates by using the DI method than the DRI method, especially over polluted eastern China (Figure S3 in the supporting information). As shown in Figure 5 (top row), the a posteriori $NO_x$ emission estimates are significantly higher with GOME-2 than OMI measurements (20–60% over high-emission regions) when the DI method is applied. In comparison, the difference are significantly lower (0–20% over high-emission regions) when the DRI method is applied. The large positive bias of GOME-2 over OMI based estimates is much reduced.

The average a posteriori anthropogenic $NO_x$ emission over China is 6.9 Tg N/yr with the DRI method, and the difference between using GOME-2 and OMI measurements is 0.4 Tg N/yr. In comparison, the OMI and GOME-2 difference between using the DI method with KNMI DOMINO2 and TM4NO2A products is significantly larger at 1.3 Tg N/yr. Considering the uncertainties in satellite measurements, retrieval, and model simulations, these results suggest that the inversion results using the measurements of OMI and GOME-2 are highly consistent when the DRI method is applied in inverse modeling.

In Figure 5 (bottom row), we compared simulated daytime tropospheric $NO_2$ VCDs by the DRI and DI methods with GOME-2 and OMI measurements. Simulated tropospheric $NO_2$ VCDs are similar to the spatial distribution of satellite-retrieved VCDs over China. More importantly, simulated daytime tropospheric $NO_2$ columns show much smaller differences between OMI and GOME-2 based results by using the DRI than DI method. On average, the simulated column difference decreased from 30% to 7% over eastern China. The high column bias of GOME-2 based results compared to those of OMI is much smaller in the DRI than DI method.

### 3.2. Seasonal Variation of Surface Anthropogenic $NO_x$ Emissions in China

Figure 6 shows the monthly surface anthropogenic $NO_x$ emission estimates using the DI and DRI methods with OMI and GOME-2 measurements. The relative differences between the two satellite data based emissions using DI and DRI methods have been shown in Figure 4. As shown in Figure 5, the a posteriori emission estimates using the DI method with GOME-2 measurements are noticeably higher than those with OMI measurements. The newly developed DRI method, on the other hand, gives fairly consistent emission estimates with GOME-2 and OMI measurements, well within the a posteriori uncertainties.

The seasonal variation of anthropogenic $NO_x$ emissions has been investigated previously using satellite $NO_2$ measurements [e.g., *Jaegle et al.*, 2005; *Miyazaki et al.*, 2012]. The DRI emission estimates with GOME-2 and OMI measurements show similar seasonal variations (Figure 6). The largest variation is seen in February compared to January and May. The decrease of emissions in February is likely associated with the Chinese New Year holidays. Lower emissions in March to May probably reflect the lower energy consumption associated with transition of heating in winter and cooling in summer. A decrease of emissions to a lesser degree is seen in September and October probably for similar reasons as in spring, although this decrease is masked by the uncertainty of emission estimate. A longer term inverse modeling study is necessary to investigate if the spring and fall decrease pattern persists from year to year. We note here that the significant

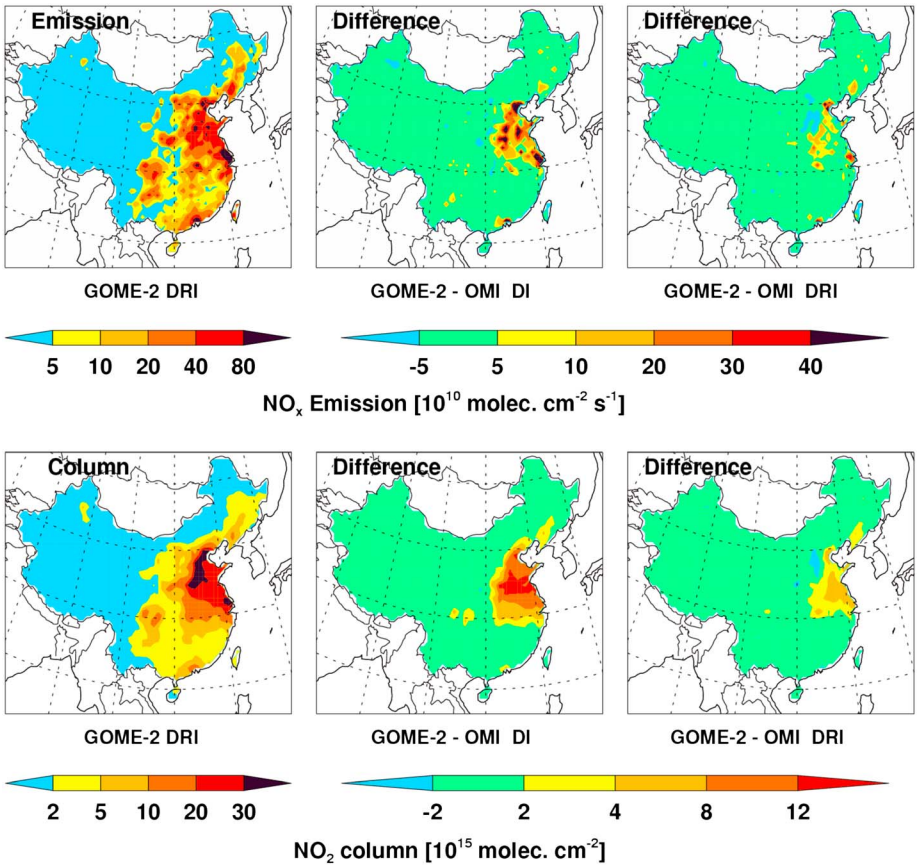


**Figure 5.** (top row) Annual mean a posteriori $NO_x$ emission estimates by using the (top, left) DRI method with GOME-2 measurements, and the differences of annual mean a posteriori $NO_x$ emission estimates between using GOME-2 and OMI measurements by using the (top, middle) DI and (top, right) DRI methods, over China for 2011. (bottom row) Annual mean simulated daytime tropospheric $NO_2$ VCDs by using (bottom, left) GOME-2 measurements, and the difference of simulated annual mean daytime tropospheric $NO_2$ VCDs between using GOME-2 and OMI measurement based emission estimates by the (bottom, middle) DI and (bottom, right) DRI methods, over China for 2011.

reduction of emission estimate difference in spring and fall using the DRI than DI method (Figure 4) is critical for discerning the seasonal change of emissions based on satellite measurements. The seasonal pattern of high emissions in winter and low emissions in spring are similar to the bottom-up estimate by *Zhang et al.* [2007], but the emission ratio of 1.4 of December and January to April and May found in this work is higher than that study.

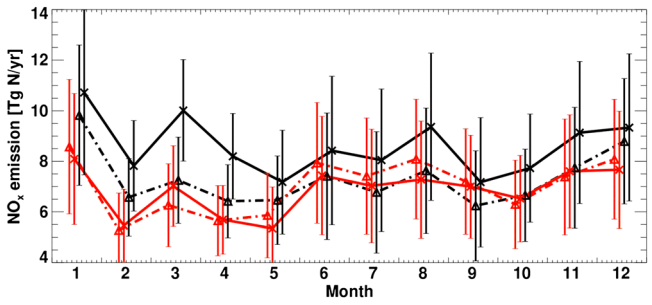


**Figure 6.** Monthly anthropogenic $NO_x$ emissions estimates by the DRI (red lines) and DI (black lines) methods with OMI (triangles, dashed lines) and GOME-2 (crosses, solid lines) measurements over China for 2011. The vertical bars show 1σ uncertainties.

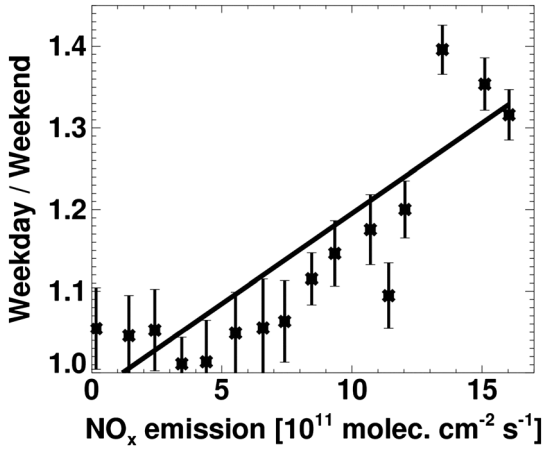


**Figure 7.** Weekday (Monday–Friday) to weekend (Saturday and Sunday) ratio of anthropogenic $NO_x$ emissions as a function of $NO_x$ emission rate over China for 2011. A vertical bar shows the 1σ uncertainty within each emission bin of $10^{11}$ molecules $cm^{-2}\,s^{-1}$. A least squares regression is shown by the black line.

### 3.3. Weekday to Weekend Emission Ratios

A significant weekly cycle of satellite observed $NO_2$ columns with a minimum value in weekend was found in urban regions in the USA, Europe, the Middle East, and Japan [e.g., *Beirle et al.*, 2003; *Boersma et al.*, 2009; *Choi et al.*, 2012; *Kaynak et al.*, 2009]. In contrast, no clear weekend effect was found in cities of China from satellite measurements [*Beirle et al.*, 2003; *Hayn et al.*, 2009]. In our analysis, we find a clearer weekday (Monday-Friday) to weekend (Saturday and Sunday) change signal using the inverse modeling results from the DRI method compared to the DI method with both GOME-2 and OMI measurements. In particular, the weekday to weekend emission ratio tends to be higher over high emission regions. We show the increase of this ratio with anthropogenic $NO_x$ emission in Figure 7. The ratio is up to the range of 1.3–1.4, which is similar to a ratio of 1.2–1.5 in urban regions of the U.S. and Europe given in previous studies [*Beirle et al.*, 2003; *Choi et al.*, 2012; *Hayn et al.*, 2009; *Kaynak et al.*, 2009]. For regions with $NO_x$ emissions $< 8\times10^{11}$ molecules $cm^{-2}\,s^{-1}$, the weekday to weekend emission ratio is close to 1, in agreement with previous analyses.

## 4. Conclusions

We improve the daily inversion of $NO_x$ emissions by updating the emissions with the inversion results and subsequently the a priori $NO_2$ profiles used in satellite retrieval on a daily basis. The newly developed DRI method therefore ensures consistency between $NO_x$ emission estimates and the $NO_2$ profiles used in satellite retrievals in a single modeling framework. We applied the methods to inverse modeling of anthropogenic $NO_x$ emissions over China using GOME-2 and OMI $NO_2$ column measurements in 2011. The high bias of GOME-2 based emission estimates relative to those based on OMI measurements in the DI method is largely removed in the DRI method. The DRI method significantly reduces the difference of anthropogenic $NO_x$ emission estimates between GOME-2 and OMI data based inversions to 0.3 Tg N/yr from 1.3 Tg N/yr using the DI method. The average emission rate of anthropogenic $NO_x$ is 6.9 Tg/yr over China in 2011. We examine the seasonal and weekly anthropogenic $NO_x$ emission variations in China using the DRI emission estimates. Anthropogenic $NO_x$ emissions are lower in spring (possibly in the fall) than winter and summer. The emission ratio from December and January to April and May is 1.4, while the peak winter and summer month emissions are similar. The weekday to weekend emission ratio tends to increase with $NO_x$ emissions, to the range of 1.3–1.4 in high $NO_x$ emission regions, similar to those previously found in urban regions of the U.S. and Europe. In low and moderate emission regions ($<8\times10^{11}$ molecules $cm^{-2}\,s^{-1}$), the weekday to weekend emission ratio is close to 1.

**Acknowledgments**
The data of DOMINO2 OMI and TM4NO2A GOME-2 SCD and tropospheric VCD products for this paper were obtained from KNMI, and we acknowledge the free use of the OMI and GOME-2 data and products from www.temis.nl. This work was supported by the NSF Atmospheric Chemistry and NASA ACMAP Programs. K. Folkert Boersma acknowledges funding by the Netherlands Organization for Scientific Research, NOW Vidi grant 864.09.001.

## References

Beirle, S., U. Platt, M. Wenig, and T. Wagner (2003), Weekly cycle of $NO_2$ by GOME measurements: A signature of anthropogenic sources, *Atmos. Chem. Phys.*, *3*, 2225–2232.

Bey, I., D. J. Jacob, R. M. Yantosca, J. A. Logan, B. D. Field, A. M. Fiore, Q. B. Li, H. G. Y. Liu, L. J. Mickley, and M. G. Schultz (2001), Global modeling of tropospheric chemistry with assimilated meteorology: Model description and evaluation, *J. Geophys. Res.*, *106*(D19), 23,073–23,095, doi:10.1029/2001JD000807.

Boersma, K. F., H. J. Eskes, and E. J. Brinksma (2004), Error analysis for tropospheric $NO_2$ retrieval from space, *J. Geophys. Res.*, *109*, D04311, doi:10.1029/2003JD003962.

Boersma, K. F., et al. (2007), Near-real time retrieval of tropospheric $NO_2$ from OMI, *Atmos. Chem. Phys.*, *7*(8), 2103–2118.

Boersma, K. F., D. J. Jacob, M. Trainic, Y. Rudich, I. DeSmedt, R. Dirksen, and H. J. Eskes (2009), Validation of urban $NO_2$ concentrations and their diurnal and seasonal variations observed from the SCIAMACHY and OMI sensors using in situ surface measurements in Israeli cities, *Atmos. Chem. Phys.*, *9*(12), 3867–3879.

Boersma, K. F., et al. (2011), An improved tropospheric $NO_2$ column retrieval algorithm for the ozone monitoring instrument, *Atmos. Meas. Tech.*, *4*(9), 1905–1928.

Choi, Y., Y. H. Wang, T. Zeng, R. V. Martin, T. P. Kurosu, and K. Chance (2005), Evidence of lightning $NO_x$ and convective transport of pollutants in satellite observations over North America, *Geophys. Res. Lett.*, *32*, L02805, doi:10.1029/2004GL021436.

Choi, Y., Y. Wang, T. Zeng, D. Cunnold, E. S. Yang, R. Martin, K. Chance, V. Thouret, and E. Edgerton (2008a), Springtime transitions of $NO_2$, CO, and $O_3$ over North America: Model evaluation and analysis, *J. Geophys. Res.*, *113*, D20311, doi:10.1029/2007JD009632.

Choi, Y., Y. H. Wang, Q. Yang, D. Cunnold, T. Zeng, C. Shim, M. Luo, A. Eldering, E. Bucsela, and J. Gleason (2008b), Spring to summer northward migration of high $O_3$ over the western North Atlantic, *Geophys. Res. Lett.*, *35*, L04818, doi:10.1029/2007GL032276.

Choi, Y., H. Kim, D. Tong, and P. Lee (2012), Summertime weekly cycles of observed and modeled $NO_x$ and $O_3$ concentrations as a function of satellite-derived ozone production sensitivity and land use types over the Continental United States, *Atmos. Chem. Phys.*, *12*(14), 6291–6307.

Ghude, S. D., R. J. Van der A, G. Beig, S. Fadnavis, and S. D. Polade (2009), Satellite derived trends in $NO_2$ over the major global hotspot regions during the past decade and their inter-comparison, *Environ. Pollut.*, *157*(6), 1873–1878.

Gu, D., Y. Wang, C. Smeltzer, and Z. Liu (2013), Reduction in $NO_x$ emission trends over China: Regional and seasonal variations, *Environ. Sci. Technol.*, *47*(22), 12,912–12,919.

Hains, J. C., et al. (2010), Testing and improving OMI DOMINO tropospheric $NO_2$ using observations from the DANDELIONS and INTEX-B validation campaigns, *J. Geophys. Res.*, *115*, D05301, doi:10.1029/2009JD012399.

Han, K. M., C. H. Song, H. J. Ahn, R. S. Park, J. H. Woo, C. K. Lee, A. Richter, J. P. Burrows, J. Y. Kim, and J. H. Hong (2009), Investigation of $NO_x$ emissions and $NO_x$-related chemistry in East Asia using CMAQ-predicted and GOME-derived $NO_2$ columns, *Atmos. Chem. Phys.*, *9*(3), 1017–1036.

Hayn, M., S. Beirle, F. A. Hamprecht, U. Platt, B. H. Menze, and T. Wagner (2009), Analysing spatio-temporal patterns of the global $NO_2$-distribution retrieved from GOME satellite observations using a generalized additive model, *Atmos. Chem. Phys.*, *9*(17), 6459–6477.

He, Y., I. Uno, Z. Wang, T. Ohara, N. Sugirnoto, A. Shimizu, A. Richter, and J. P. Burrows (2007), Variations of the increasing trend of tropospheric $NO_2$ over central east China during the past decade, *Atmos. Environ.*, *41*(23), 4865–4876.

Irie, H., K. F. Boersma, Y. Kanaya, H. Takashima, X. Pan, and Z. F. Wang (2012), Quantitative bias estimates for tropospheric $NO_2$ columns retrieved from SCIAMACHY, OMI, and GOME-2 using a common standard for East Asia, *Atmos. Meas. Tech.*, *5*(10), 2403–2411.

Jaegle, L., L. Steinberger, R. V. Martin, and K. Chance (2005), Global partitioning of $NO_x$ sources using satellite observations: Relative roles of fossil fuel combustion, biomass burning and soil emissions, *Faraday Discuss.*, *130*, 407–423.

Jing, P., D. Cunnold, Y. Choi, and Y. Wang (2006), Summertime tropospheric ozone columns from Aura OMI/MLS measurements versus regional model results over the United States, *Geophys. Res. Lett.*, *33*, L17817, doi:10.1029/2006GL026473.

Kaynak, B., Y. Hu, R. V. Martin, C. E. Sioris, and A. G. Russell (2009), Comparison of weekly cycle of $NO_2$ satellite retrievals and $NO_x$ emission inventories for the continental United States, *J. Geophys. Res.*, *114*, D05302, doi:10.1029/2008JD010714.

Kunhikrishnan, T., M. G. Lawrence, R. von Kuhlmann, A. Richter, A. Ladstatter-Weissenmayer, and J. P. Burrows (2004), Analysis of tropospheric $NO_x$ over Asia using the model of atmospheric transport and chemistry (MATCH-MPIC) and GOME-satellite observations, *Atmos. Environ.*, *38*(4), 581–596.

Kurokawa, J., K. Yumimoto, I. Uno, and T. Ohara (2009), Adjoint inverse modeling of $NO_x$ emissions over eastern China using satellite observations of $NO_2$ vertical column densities, *Atmos. Environ.*, *43*(11), 1878–1887.

Levelt, P. F., E. Hilsenrath, G. W. Leppelmeier, G. H. J. van den Oord, P. K. Bhartia, J. Tamminen, J. F. de Haan, and J. P. Veefkind (2006), Science objectives of the ozone monitoring instrument, *IEEE Trans. Geosci. Remote Sens.*, *44*(5), 1199–1208.

Lin, J. T., M. B. McElroy, and K. F. Boersma (2010), Constraint of anthropogenic $NO_x$ emissions in China from different sectors: A new methodology using multiple satellite retrievals, *Atmos. Chem. Phys.*, *10*(1), 63–78.

Lin, J. T., Z. Liu, Q. Zhang, H. Liu, J. Mao, and G. Zhuang (2012), Modeling uncertainties for tropospheric nitrogen dioxide columns affecting satellite-based inverse modeling of nitrogen oxides emissions, *Atmos. Chem. Phys.*, *12*(24), 12,255–12,275.

Liu, Z., et al. (2010), Evidence of reactive aromatics as a major source of peroxy acetyl nitrate over China, *Environ. Sci. Technol.*, *44*(18), 7017–7022.

Liu, Z., et al. (2012a), Exploring the missing source of glyoxal (CHOCHO) over China, *Geophys. Res. Lett.*, *39*, L10812, doi:10.1029/2012GL051645.

Liu, Z., et al. (2012b), Summertime photochemistry during CAREBeijing-2007: $RO_x$ budgets and $O_3$ formation, *Atmos. Chem. Phys.*, *12*(16), 7737–7752.

Ma, J. Z., A. Richter, J. P. Burrows, H. Nuss, and J. A. van Aardenne (2006), Comparison of model-simulated tropospheric $NO_2$ over China with GOME-satellite data, *Atmos. Environ.*, *40*(4), 593–604.

Martin, R. V., D. J. Jacob, K. Chance, T. P. Kurosu, P. I. Palmer, and M. J. Evans (2003), Global inventory of nitrogen oxide emissions constrained by space-based observations of $NO_2$ columns, *J. Geophys. Res.*, *108*(D17), 4537, doi:10.1029/2003JD003453.

Miyazaki, K., H. J. Eskes, and K. Sudo (2012), Global $NO_x$ emission estimates derived from an assimilation of OMI tropospheric $NO_2$ columns, *Atmos. Chem. Phys.*, *12*(5), 2263–2288.

Ohara, T., H. Akimoto, J. Kurokawa, N. Horii, K. Yamaji, X. Yan, and T. Hayasaka (2007), An Asian emission inventory of anthropogenic emission sources for the period 1980–2020, *Atmos. Chem. Phys.*, *7*(16), 4419–4444.

Richter, A., V. Eyring, J. P. Burrows, H. Bovensmann, A. Lauer, B. Sierk, and P. J. Crutzen (2004), Satellite measurements of $NO_2$ from international shipping emissions, *Geophys. Res. Lett.*, *31*, L23110, doi:10.1029/2004GL020822.

Richter, A., J. P. Burrows, H. Nuss, C. Granier, and U. Niemeier (2005), Increase in tropospheric nitrogen dioxide over China observed from space, *Nature*, *437*(7055), 129–132.

Shi, C. N., H. J. S. Fernando, Z. F. Wang, X. Q. An, and Q. Z. Wu (2008), Tropospheric $NO_2$ columns over East Central China: Comparisons between SCIAMACHY measurements and nested CMAQ simulations, *Atmos. Environ.*, *42*(30), 7165–7173.

Stavrakou, T., J. F. Muller, K. F. Boersma, I. De Smedt, and R. J. van der A (2008), Assessing the distribution and growth rates of $NO_x$ emission sources by inverting a 10-year record of $NO_2$ satellite columns, *Geophys. Res. Lett.*, *35*, L10801, doi:10.1029/2008GL033521.

Streets, D. G., et al. (2003), An inventory of gaseous and primary aerosol emissions in Asia in the year 2000, *J. Geophys. Res.*, *108*(D21), 8809, doi:10.1029/2002JD003093.

Uno, I., et al. (2007), Systematic analysis of interannual and seasonal variations of model-simulated tropospheric $NO_2$ in Asia and comparison with GOME-satellite data, *Atmos. Chem. Phys.*, *7*(6), 1671–1681.

van der A, R. J., D. Peters, H. Eskes, K. F. Boersma, M. Van Roozendael, I. De Smedt, and H. M. Kelder (2006), Detection of the trend and seasonal variation in tropospheric $NO_2$ over China, *J. Geophys. Res.*, *111*, D12317, doi:10.1029/2005JD006594.

Vinken, G. C. M., K. F. Boersma, A. van Donkelaar, and L. Zhang (2014), Constraints on ship $NO_x$ emissions in Europe using GEOS-Chem and OMI satellite $NO_2$ observations, *Atmos. Chem. Phys.*, *14*(3), 1353–1369.

Wang, Y. H., Y. S. Choi, T. Zeng, B. Ridley, N. Blake, D. Blake, and F. Flocke (2006), Late-spring increase of trans-Pacific pollution transport in the upper troposphere, *Geophys. Res. Lett.*, *33*, L01811, doi:10.1029/2005GL024975.

Wang, Y., Y. Choi, T. Zeng, D. Davis, M. Buhr, L. G. Huey, and W. Neff (2007), Assessing the photochemical impact of snow $NO_x$ emissions over Antarctica during ANTCI 2003, *Atmos. Environ.*, *41*(19), 3944–3958.

Yang, Q., Y. Wang, C. Zhao, W. Gustafson, and M. Shao (2011), $NO_x$ emission reduction and its effects on ozone during the 2008 Olympic games, *Environ. Sci. Tech.*, *45*(4), 6404–6410.

Zeng, T., Y. H. Wang, K. Chance, E. V. Browell, B. A. Ridley, and E. L. Atlas (2003), Widespread persistent near-surface ozone depletion at northern high latitudes in spring, *Geophys. Res. Lett.*, *30*(24), 2298, doi:10.1029/2003GL018587.

Zeng, T., Y. Wang, K. Chance, N. Blake, D. Blake, and B. Ridley (2006), Halogen-driven low-altitude $O_3$ and hydrocarbon losses in spring at northern high latitudes, *J. Geophys. Res.*, *111*, D17313, doi:10.1029/2005JD006706.

Zhang, Q., et al. (2007), $NO_x$ emission trends for China, 1995–2004: The view from the ground and the view from space, *J. Geophys. Res.*, *112*, D22306, doi:10.1029/2007JD008684.

Zhang, Q., et al. (2009), Asian emissions in 2006 for the NASA INTEX-B mission, *Atmos. Chem. Phys.*, *9*(14), 5131–5153.

Zhang, Q., G. N. Geng, S. W. Wang, A. Richter, and K. B. He (2012), Satellite remote sensing of changes in $NO_x$ emissions over China during 1996–2010, *Chin. Sci. Bull.*, *57*(22), 2857–2864.

Zhao, C., and Y. Wang (2009), Assimilated inversion of $NO_x$ emissions over east Asia using OMI $NO_2$ column measurements, *Geophys. Res. Lett.*, *36*, L06805, doi:10.1029/2008GL037123.

Zhao, C., Y. H. Wang, and T. Zeng (2009a), East China plains: A "basin" of ozone pollution, *Environ. Sci. Technol.*, *43*(6), 1911–1915.

Zhao, C., Y. Wang, Y. Choi, and T. Zeng (2009b), Summertime impact of convective transport and lightning $NO_x$ production over North America: Modeling dependence on meteorological simulations, *Atmos. Chem. Phys.*, *9*(13), 4315–4327.

Zhao, C., Y. Wang, Q. Yang, R. Fu, D. Cunnold, and Y. Choi (2010), Impact of East Asian summer monsoon on the air quality over China: View from space, *J. Geophys. Res.*, *115*, D09301, doi:10.1029/2009JD012745.